Anisotropy of nanoscale friction: Influence of lattice structure, temperature, and wear

Jennifer Konrad,[1,*] Enrico Gnecco,[2,*,†] Dirk Dietzel,[1,3] and André Schirmeisen[1,3,‡]

[1]*Institute of Applied Physics (IAP), Justus-Liebig-Universität Giessen, 35392 Giessen, Germany*

[2]*Marian Smoluchowski Institute of Physics, Jagiellonian University, 30348 Krakow, Poland*

[3]*Center for Materials Research, Justus-Liebig-Universität Giessen, 35392 Giessen, Germany*

(Received 18 January 2023; accepted 20 April 2023; published 30 May 2023)

The anisotropy of nanoscale friction is analyzed for different samples using friction force microscopy under ultrahigh-vacuum conditions with varying scan directions. For both MoS_2 and highly oriented pyrolytic graphite surfaces, our experiments reveal a sixfold symmetry of the friction vector plots in accordance with solutions of the Langevin equation, where the atomic force microscope tip is treated as a point mass elastically driven on the hexagonal surface lattices. In addition, the effect of temperature is analyzed both by experiment and by simulations. In both cases we find that increased temperature not only lowers the absolute friction values but also decreases the friction anisotropy. In contrast, experiments on NaCl cannot be explained on a similar basis. While the square symmetry is clearly revealed in the first measurements, it progressively deteriorates with repeated scanning, which is possibly due to abrasive wear occurring at the interface.

DOI: 10.1103/PhysRevB.107.195438

I. INTRODUCTION

Sliding friction on the nanometer scale presents peculiar features, such as, e.g., atomic stick slip [1], with no equivalent macroscopic counterparts. Understanding atomic-scale friction has thus long since been one of the primary objectives in nanotribology. Experimental investigations are routinely performed using atomic force microscopy (AFM), but significant information is still lacking in specific contexts such as the characterization of atomic-scale friction at low temperatures.

In this context, AFM experiments allow us to analyze the model case of a single nanoscale asperity sliding on a solid surface. In spite of the continuous formation and rupture of chemical bonds at the interface [2–5], the atoms in the contact area form a well-defined patch given by the shape of the tip apex. When the contacting materials are sheared past each other, the patch moves discontinuously along the surface in a series of stick-slip events. This process is usually well described by the Prandtl-Tomlinson model, where the tip is assumed to be elastically driven through an effective potential interaction reproducing its interaction with the sample surface [6,7].

When the driving spring force is zero, the atoms in the contact patch simply oscillate around their equilibrium positions. If the interaction is strong enough, i.e., if the contact is not "superlubric" [8,9], the average configuration of the patch barely changes when the spring support is pulled and the spring force increases. When a critical elongation of the spring is reached, the equilibrium becomes suddenly unstable, and the tip slips. The slip motion is, in most cases, strongly damped by the kinetic friction, bringing the tip to a new rest position in a very short time (as compared with the duration of the stick phase).

On a crystalline surface the slip distance and orientation are defined by the size and symmetry of the unit cells of the surface lattice. The slip usually ends in an adjacent location on the lattice, but longer slips are also possible if the loading force is high and/or the damping coefficient of the oscillations is sufficiently low [10,11]. The situation is more complicated in a humid environment, where capillary bridges can increase or even dominate the adhesion at the interface [12–14], but this case is not considered here.

In recent years, the directional dependence of nanoscale friction has, in particular, received increased interest [8,15–23], not only to understand the phenomenon of superlubricity but also motivated by the goal of understanding the fundamental stick-slip process in full detail. Note that this aspect was not considered in the seminal work by Prandtl [6].

Regarding the direction of each slip, the main crystallographic directions are preferred, meaning that the tip will follow a zigzag pathway if the scan direction is arbitrarily oriented [15,19]. As a consequence, the average value of the spring force component along this direction, which can be identified with the friction force F hindering the tip motion, depends on the angle ϕ between the pulling direction and a given crystallographic direction on the surface lattice.

Analytical expressions have been derived for the $F(\phi)$ relation on simple square and hexagonal surface lattices [15,19]. These expressions are strictly valid if the slider can be represented as a point mass. This is not the case if it is also crystalline, as is, e.g., the case for graphite flakes attached to the tip [8,16,24]. For amorphous configurations at the tip termination one has to rely on molecular dynamics (MD). As an example, MD simulations by Vazirisereshk *et al.* showed on MoS_2 [20] how tip-induced changes in the potential energy surface can modify the symmetry of the system in a way that experiments under ultrahigh-vacuum (UHV) conditions reveal

*These authors contributed equally to this work.
†enrico.gnecco@uj.edu.pl
‡schirmeisen@ap.physik.uni-giessen.de

a twofold symmetry rather than the 60° symmetry normally expected for the hexagonal MoS_2 lattice.

However, in spite of the simplicity of the problem, experimental investigations of friction anisotropy on the nanoscale are still scarce. One reason is that the zigzag motion of the tip introduces a second component in the spring force perpendicular to the scan direction. The design of the cantilever force sensors that is usually adopted for these measurements implies that the corresponding spring constant is not the same as the spring constant of the force component parallel to the scan direction. Apart from building specialized cantilevers [8], one way to solve the problem is rotating the sample surface, but this is only feasible in a vacuum by unconventional dedicated setups [19].

Here, we apply an alternative solution to bypass the problem by running preliminary measurements on an isotropic SiO_2 surface with scan direction changed in steps of $\Delta\phi = 1°$. From the results taken as a reference for calibrating friction forces with arbitrary scan directions, we could validate friction anisotropy as predicted by the Prandtl-Tomlinson model on two surfaces with hexagonal symmetry: MoS_2 and highly oriented pyrolytic graphite (HOPG). In the first case, our UHV experiments confirm the occurrence of 60° symmetry (similar to graphite surfaces [15]) both in the friction vector plot and in stick-slip curves expected from numeric simulations with a pointlike tip and in contrast with recent reports assuming a twofold symmetry induced by the tip apex [17,20]. On HOPG, we extend the validation of friction anisotropy predicted by the Prandtl-Tomlinson mode to low temperatures down to 100 K. In this case, increasing effects of thermal activation [25,26] lead to a less-defined directional dependence in the experiments and also numerical simulations. A similar analysis was performed on the square lattice of NaCl. In spite of the basic square structure of the friction vector plots observed in the first measurements, which appears to be consistent with the friction vector plots expected in the frame of the Prandtl-Tomlinson model, stick-slip was not detected. Furthermore, the square pattern was progressively lost during repetition of the measurements at different angles. This points towards the occurrence of significant wear on the alkali halide surfaces, as confirmed by postprocess AFM overviews of the scanned area.

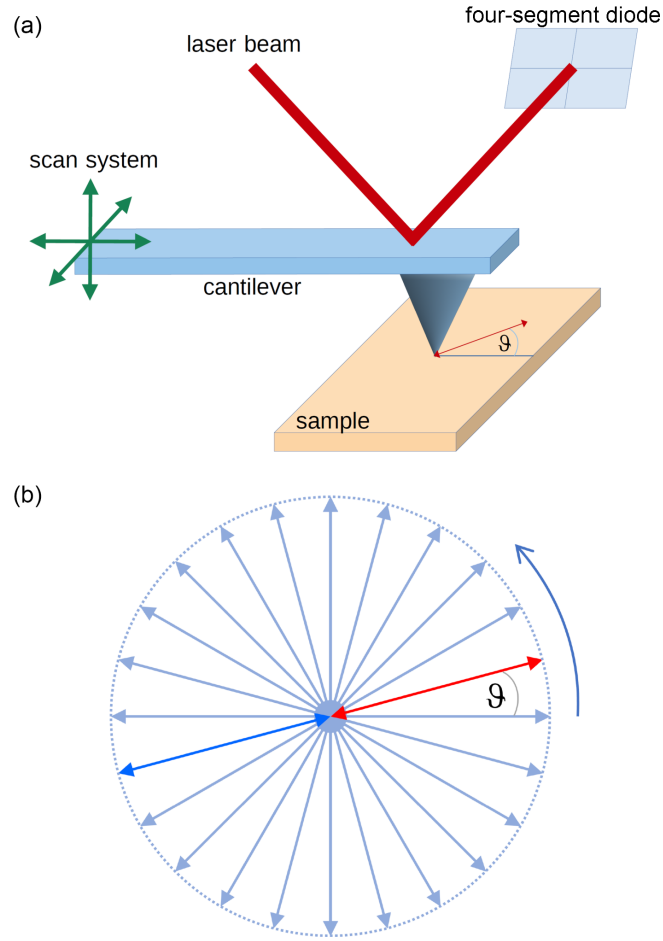

FIG. 1. Setup and experimental protocol to measure friction as a function of sliding direction. (a) A conventional beam-deflection AFM in contact mode operation is used for friction measurement. To probe different directions, the cantilever is moved back and forth along straight lines under varying angles ϑ. (b) Scheme of the procedure to measure friction as a function of sliding direction. Friction loops originating from the same starting point are recorded. The sliding angle ϑ is gradually increased in the counterclockwise direction (please note that the figure shows 15° steps, while 1° steps were used in the actual experiments). Angles differing by 180° (e.g., indicated by the red and dark blue arrows) are essentially probing the same tribological configuration.

II. EXPERIMENTAL APPROACH AND NUMERICAL SIMULATIONS

A. Experimental approach

All experiments have been performed using a variable-temperature atomic force microscope (VT-AFM) from Scienta Omicron under UHV conditions in contact mode operation at a base pressure of about 5×10^{-10} mbar. In this setup, the temperature was varied between 100 K and room temperature using liquid nitrogen as coolant in a tunable flow cryostat. In all our AFM experiments the surfaces were analyzed by soft silicon cantilevers with a normal force constant of 0.2 N/m and a free resonance frequency of ∼23 kHz (LFMR; Nanosensors). As samples we used freshly cleaved surfaces of highly oriented pyrolytic graphite (HOPG), molybdenum disulfide [MoS_2(0001)], and sodium chloride [NaCl(001)]. Sodium chloride is characterized by an fcc structure and fourfold symmetry, while the graphene layers of HOPG are described by their hexagonal honeycomb structure and a sixfold symmetry. The layers of MoS_2(0001), on the other hand, only show a threefold symmetry since a top view reveals a hexagonal structure where Mo and S are alternating. Before the experiments, all samples were heated to 200 °C under UHV conditions for 1.5 h in order to remove adsorbates from the surfaces.

To probe the influence of the sliding direction on friction, we recorded a series of friction loops starting at the same point of origin but wherein angle ϑ, which defines the scan direction, was changed in the counterclockwise direction by steps of 1° (Fig. 1). In this configuration, the friction signal is no longer detected solely as the typical left-right signal

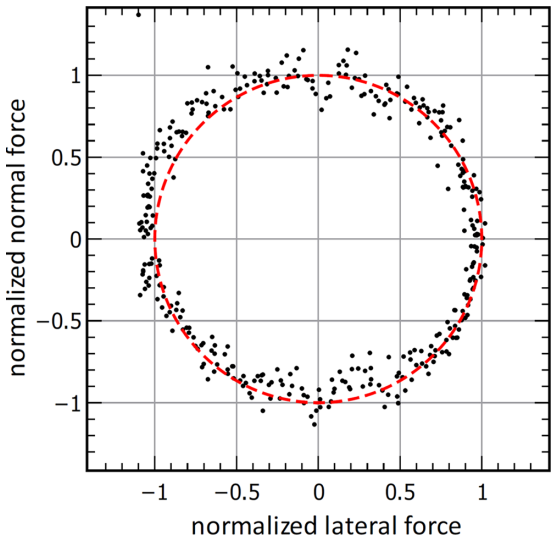

FIG. 2. Normalized friction vector plot obtained on an amorphous SiO_2 surface. After the normalization the black data points measured with an angular resolution of 1° can be well approximated by a circle with radius $r = 1$ (dashed red line). In addition, we find that the black data points show an even angular distribution, as is expected for an amorphous surface with friction vectors directly opposite to the sliding direction.

of a four-segment photodetector F_{FL} [1,27,28], but instead, a second signal component F_{FN} arises from movement parallel to the long cantilever axis and cantilever buckling that is detected as a top-bottom voltage signal. To exclude cross talk between topography and F_{FN}, we used low feedback settings and a fast scan speed of 1 μm/s. In this case the z feedback is sufficient to compensate slow vertical drift but is ultimately too slow to interfere with the friction signal.

To test and calibrate this experimental configuration, we first analyzed the amorphous silicon dioxide layer of a Si wafer as a reference sample. For this sample, friction forces should be isotropic and directly opposite to the sliding direction [15]. Due to different sensitivities for force detection in the x and y directions the resulting vector plot for uncalibrated force signals is then found to be of elliptical shape, and the ratio of the calibration factors can be obtained by transforming the ellipsis into a circle. Figure 2 shows an exemplary friction vector plot after reshaping calibration.

In some cases, a slight rotation of the uncalibrated ellipsis can be observed. This effect can be attributed to cross talk between bending and buckling during the cantilever movement as well as to the fact that friction detection in the x and y directions is no longer fully decoupled if the long cantilever axis is not perfectly aligned with the y direction for scanning. However, also in this case, the circular shape of the friction vector plot can be obtained by compensating the rotation and considering the calibration factors for different directions.

In addition, rotations of the friction vector plot for measurements on the same material can also arise if samples are glued to the sample holder with different orientations. For better intercomparability, such rotations have been corrected for the experiments on NaCl.

B. Numerical simulations

To simulate the dependence of the lateral force signal on the sliding direction, we have solved the Langevin equation of motion for a point mass representing the apex of the AFM tip driven by an elastic spring on periodic potentials with square and hexagonal symmetries:

$$V_{sq}(x, y) = -U_0\left(\cos\frac{2\pi x}{a} + \cos\frac{2\pi y}{a}\right), \quad (1)$$

$$V_{hex}(x, y) = -U_0\left(\frac{1}{2}\cos\frac{2\pi x}{a}\cos\frac{2\pi y}{a\sqrt{3}} + \cos\frac{4\pi y}{a\sqrt{3}}\right). \quad (2)$$

In both cases, stick-slip is expected if the parameter $\eta = 4\pi^2 U_0/(ka^2) > 1$, where U_0, k, and a are the amplitude of the tip-surface interaction potential, the spring constant, and the lattice constant, respectively, with a rather complex behavior up to $\eta \approx 1.45$ on the hexagonal lattice [29]. In each run the tip was positioned at a random location close to the origin of the (x, y) plane and virtually scanned on a length $L = 10$ nm with a time step of 100 ns and the scan direction increased by 1° with respect to the previous run. The tip mass was set as $m = 10^{-12}$ kg. Following Steiner *et al.* [30], k was supposed to take the same value of 1 N/m (in our case) in the x and y directions. A damping coefficient $\gamma = 10\gamma_c$, with $\gamma_c = 2\sqrt{k/m}$, guaranteed that the tip oscillations in the slip phase are strongly damped. Thermal vibrations were introduced by means of the Ermak algorithm [31].

III. RESULTS AND DISCUSSION

In the following sections we will now focus on the influence of parameters such as surface structure, temperature, and wear on the directional dependence of friction for atomically flat surfaces. To this end, we will analyze friction on MoS_2, HOPG, and NaCl. As we will see, friction on the relatively stable surfaces of MoS_2 and HOPG is only determined by the sample temperature and the crystalline structure, while analyzing the directional friction characteristics of NaCl is complicated by the occurrence of wear during continuous measurements, which affects both the directional dependence and the magnitude of the friction forces.

A. Friction anisotropy on hexagonal lattices: MoS_2 and HOPG

In this section, the experimental approach was first applied to characterize the previously unexplored directional dependence of friction on MoS_2 before probing the temperature dependence for the case of HOPG. Figure 3(a) shows the friction vector diagram for MoS_2 measured with a scan range of 10 nm and an angular resolution of 1° over ten full rotations. The friction vector plot clearly reveals that static friction is not isotropic but, instead, the friction vectors are clustered into six groups. This result is also evident from Fig. 3(b), which shows the angular distribution of the friction vectors as a histogram between 0° and 360°. Here, six peaks with a spacing of ∼60° can clearly be identified. At first glance, this result might be surprising, since the MoS_2 substrate is, strictly speaking, only characterized by a threefold symmetry. However, any differences between directions with 60° spacing are eliminated if friction is probed by back-and-forth scanning, as is done in our experiments.

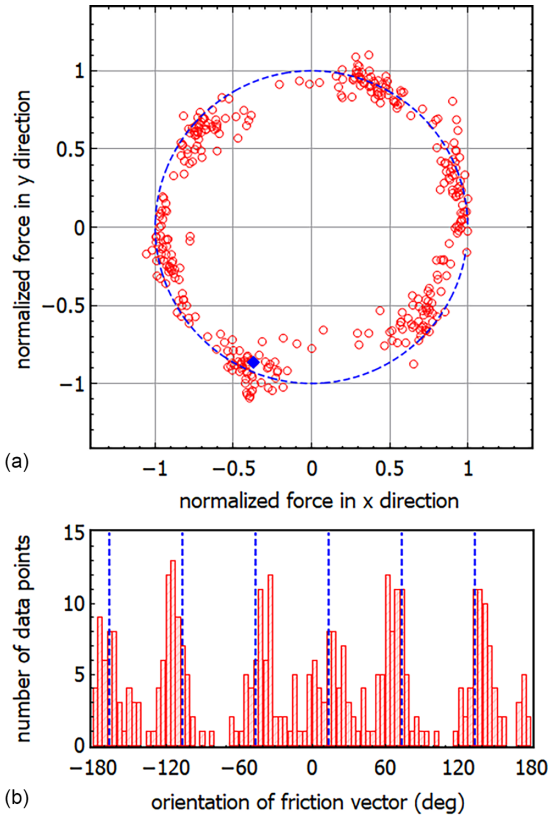

FIG. 3. Analysis of the directional dependence of friction for MoS_2 at room temperature. (a) Friction vector plot containing 360 data points as a result of averaging over ten rotations with an angular resolution of 1°. The blue data point indicates the direction corresponding to 264° (or −96°), which is further discussed in the main text. The dashed blue circle corresponds to a friction value of ∼2 nN. (b) Histogram derived from the friction vector plot with six peaks that illustrate the 60° symmetry of the friction vector plot.

Similar to the results reported by Balakrishna *et al.* on HOPG [15], preferred sliding directions can also be identified from the stick-slip pattern of the individual friction traces [Figs. 4(a)–4(f)]. For instance, one of these directions is found to be close to −96°, which roughly equals scanning downwards parallel to the long cantilever axis. Figure 4(b) shows the corresponding lateral forces when sliding close to this preferred direction. The slip length is in the range of several nanometers and can be attributed to the relatively rare jumps of the tip apex between adjacent atomic rows in a preferred direction. In the case of a sliding angle of −96°, we find approximately one slip per 6 nm of sliding, which corresponds to an angular offset of about 3°. For an angle of −98° the tip even becomes completely stuck in the *y* direction, and no slips occur for a scan length of 10 nm. Still, the resulting friction vector, as indicated by the blue diamond in Fig. 3(a), is within the cluster of friction vectors that is centered around an angle of about 244°. If we now consider sliding directions shifted by about 60°, the physical configuration essentially remains the same, but due to the alignment between cantilever and substrate, a stick-slip pattern in F_{FL} with a periodicity of about 330 pm can be observed.

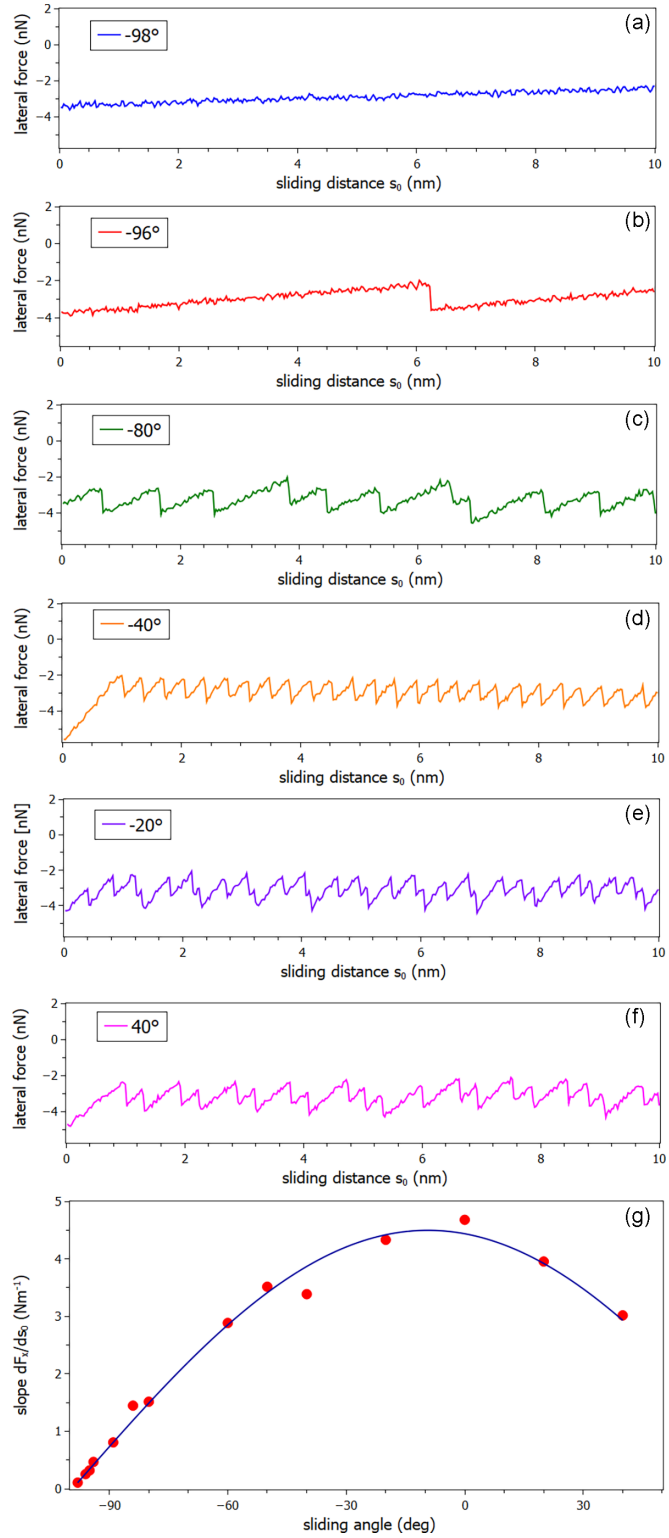

FIG. 4. Analysis of the directional dependence of friction for MoS_2 at room temperature. (a)–(f) Exemplary friction traces in F_{FL} when scanning in different directions between −98° and 40°. For the angle of −98°, the tip becomes fully stuck in the *y* direction, and no slips occur. (g) Slopes of the lateral force signal F_{FL} for the angles shown in (a)–(f) together with a function proportional to $\cos(\varphi - \varphi_0)$, with $\varphi_0 = -10°$.

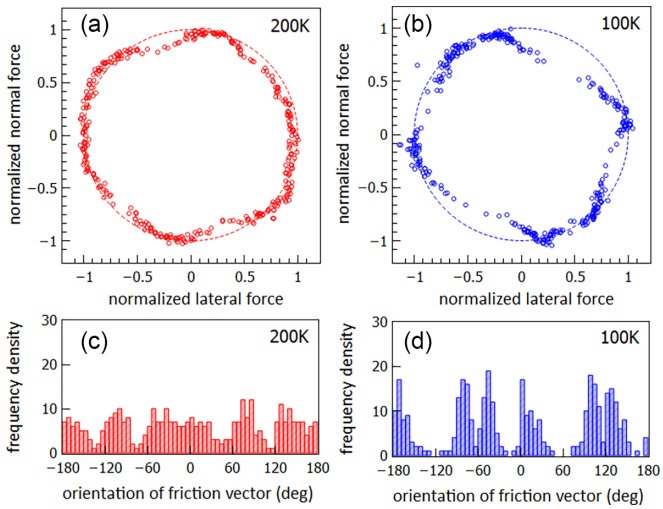

FIG. 5. Frictional anisotropy measured on HOPG for two different temperatures. (a) Friction vector plot obtained at 200 K. (b) Friction vector plot obtained at 100 K. (c) Distribution of friction directions at 200 K. (d) Distribution of friction directions at 100 K.

The evolution of F_x in the stick phase with different scan directions can be easily understood by observing that this force component is plotted, in Figs. 4(a)–4(f), as a function of $s_0 = (x_0^2 + y_0^2)^{1/2}$, where (x_0, y_0) is the support position, and not, as usual, of x_0. If the slip phase is sharp, as in the present case, we can assume that [9]

$$\frac{dF_x}{ds_0} = \frac{dF_x}{dx_0/\cos\varphi} \approx k\cos\varphi. \tag{3}$$

However, Fig. 4(g) shows that a good agreement between experiment and theoretical prediction is obtained only if the angles are measured from a value of $\varphi_0 \approx -10^\circ$. This offset can be attributed to a slight misalignment of the cantilever, which is almost unavoidable in the manual cantilever fixing procedure using epoxy glue and subsequent baking.

Interestingly, these results on MoS_2 do not show the twofold symmetry, which was recently reported in Ref. [20], but they are fully consistent with the behavior expected for a point mass on a hexagonal potential energy surface.

A further question concerns the degree of clustering in the friction vector plots. For the simplest case of a square lattice with decoupled potentials for movement in the x and y directions and a sample temperature of $T = 0$ K, it is anticipated that the friction vector plot only consists of four single points with 90° spacing [15]. A more complex behavior must be expected for hexagonal lattices at finite temperatures. Here, the influence of the sliding velocity and coupling between three preferential sliding directions should result in a less-defined clustering of the friction vectors and wider peaks in the histograms, as seen in Fig. 3.

To test this assumption, we have now performed temperature-dependent measurements of the directional dependence of friction for the case of HOPG. Figure 5 shows both the friction vector plots [Figs. 5(a) and 5(b)] and the corresponding histograms [Figs. 5(c) and 5(d)] for temperatures of 200 and 100 K. All of the panels in Fig. 5 clearly reflect the sixfold symmetry of the sample reported by Balakrishna *et al.*

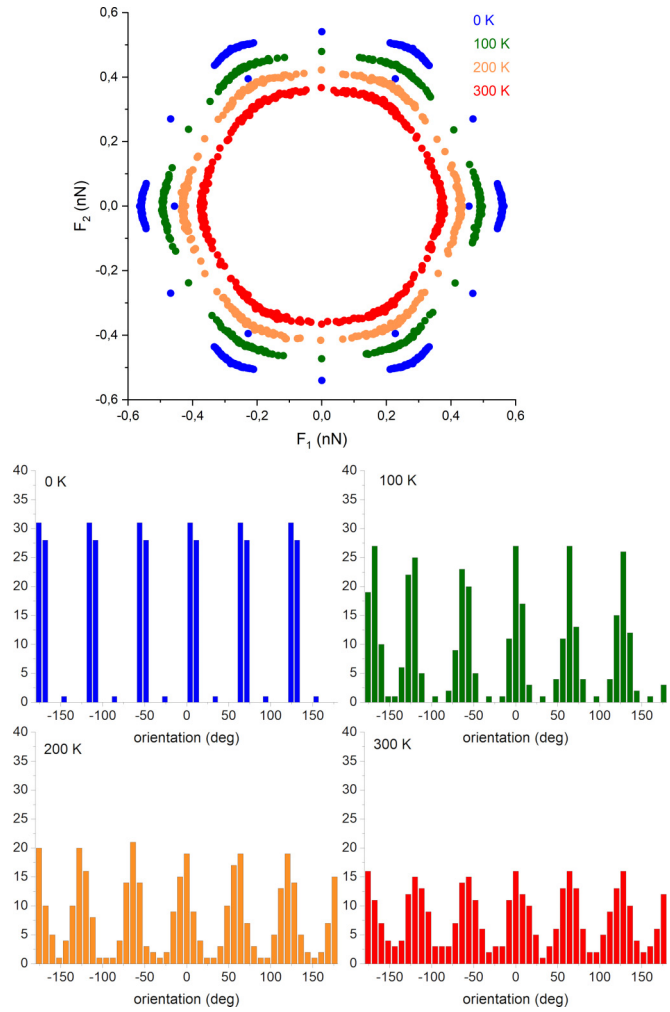

FIG. 6. Top: Simulated vector plot corresponding to the hexagonal symmetry potential given by Eq. (2) at different temperatures between 0 and 300 K. Bottom: Corresponding histograms of the angle distribution for the different temperatures.

[15]. Figures 5(a) and 5(b) are quite comparable to results at room temperature, where the zigzag directions were found to act as preferred sliding directions on HOPG [15]. In the present case, we observe that both the clusters and the peaks of Fig. 5 become more defined if the temperature is reduced, in line with the aforementioned expectations.

To validate these results, we have performed numerical simulations where the movement of the tip apex across the potential energy surface of the sample (with $U_0 = 0.2$ eV and the Mo_2 lattice constant $a = 0.315$ nm, corresponding to $\eta \approx 20$) was calculated as a function of the pulling direction at 0, 100, 200, and 300 K (top panel of Fig. 6). Here, the coordinates F_x and F_y are obtained from the components $F_\parallel$ and $F_\perp$ of the spring force along and perpendicular to the scan direction, respectively, according to the formulas $F_x = F_\parallel \cos\varphi - F_\perp \sin\varphi$ and $F_y = F_\parallel \sin\varphi + F_\perp \cos\varphi$. As a result, the data points are arranged on a hexagonal profile, which tends to shrink to a circle when the temperature is increased, with less significant clustering at 30°, 90°, and so on (top panel of Fig. 6). Note the isolated points in the zigzag and armchair directions observed at 0 K, which are consistent with the emergence of singular-

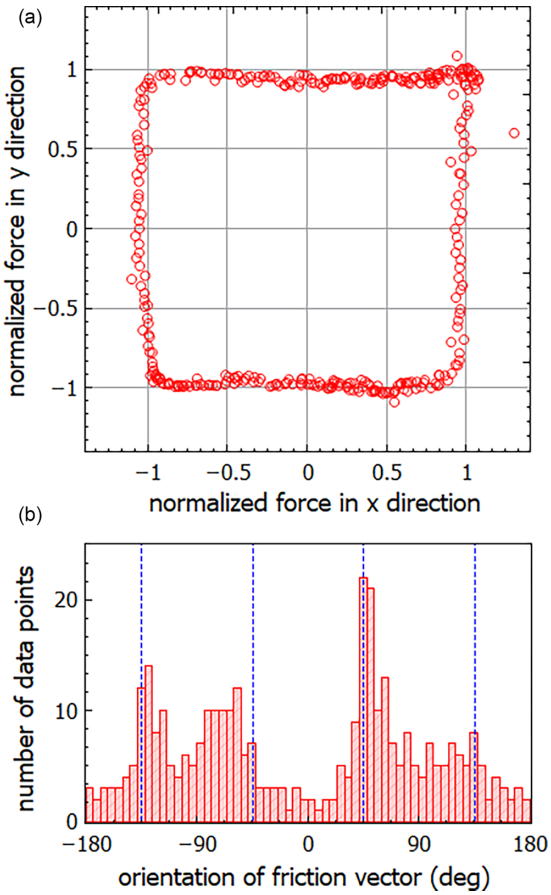

FIG. 7. Analysis of the directional dependence of friction measured on NaCl at room temperature using a scan length of 100 nm. (a) Friction vector plot containing 360 data points as a result of averaging over ten rotations with an angular resolution of 1°. (b) Histogram derived from the friction vector plot to illustrate the angular distribution of friction forces.

ities when thermal vibrations are absent [32]. These features can also be recognized in the histograms in the bottom panels of Fig. 6, confirming the higher degree of clustering at low temperature experimentally observed in Figs. 5(c) and 5(d).

B. Friction anisotropy on a square lattice: NaCl

In addition to the hexagonal structures of MoS_2 and HOPG, we have also analyzed the anisotropy of friction for a square lattice, namely, NaCl, obtained at room temperature and for a scan length of 100 nm.

Figure 7 shows both the friction vector plot [Fig. 7(a)] and the histogram of friction forces derived from it. Interestingly, from Fig. 7(a) we find that clusters of data points cannot readily be identified but instead the data points appear to be forming a more continuous square. This is corroborated by Fig. 7(b), where the histogram of friction vectors show two peaks at 45° and −135° and a rather irregular distribution in the background.

The behavior is different in simulations, where the data points are significantly clustered at 45°, 135°, etc. (see Supplemental Material [33]). Similar to the hexagonal case, the clustering is enhanced at low temperature. This trend, including the emergence of singularities when the tip is scanned along the x and y axes, is also in line with previous results [32]. While this result could be attributed to an asymmetric tip shape, the reason for the discrepancy between experiments and numerical simulations becomes more dramatic at lower temperatures. In this case, it appears that a major role is played by abrasive wear of the NaCl surface, as discussed in the next section.

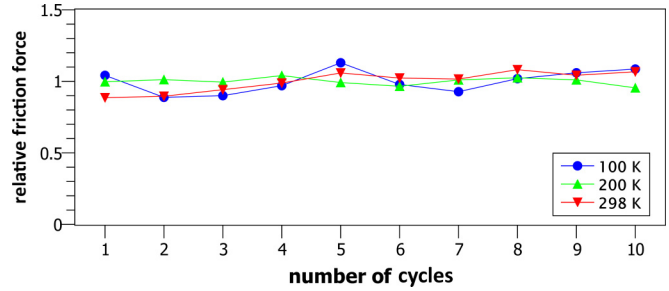

FIG. 8. Normalized average friction force per cycle measured on HOPG for three different temperatures.

C. Friction anisotropy on NaCl: Influence of wear

In the previous sections, all friction vector plots have been derived as an average over ten full cycles obtained through successive scanning at the same position. Such an approach is only possible if the sample surface is not significantly modified by the continuous scanning process and the average friction level per cycle remains constant as is exemplified for the case of HOPG in Fig. 8.

Experiments on NaCl at $T < 300$ K showed a distinct decrease of the average friction with increasing number of cycles. In Fig. 9 this is illustrated by a friction vector plot over ten full cycles obtained on NaCl at 150 K. In addition, also the development of an increasingly irregular shape of

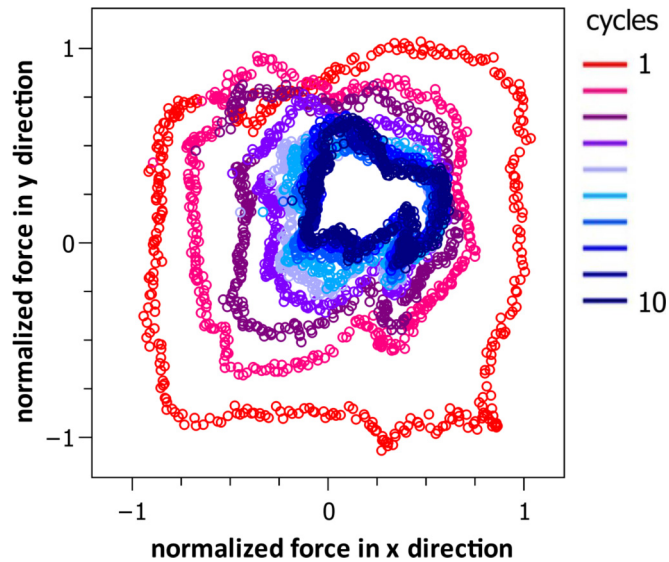

FIG. 9. Friction vector plot obtained on NaCl at $T = 150$ K as a function of the cycle number. With increasing number of cycles, the initially square shape of the friction vector plot becomes more irregular, and the average normalized friction decreases.

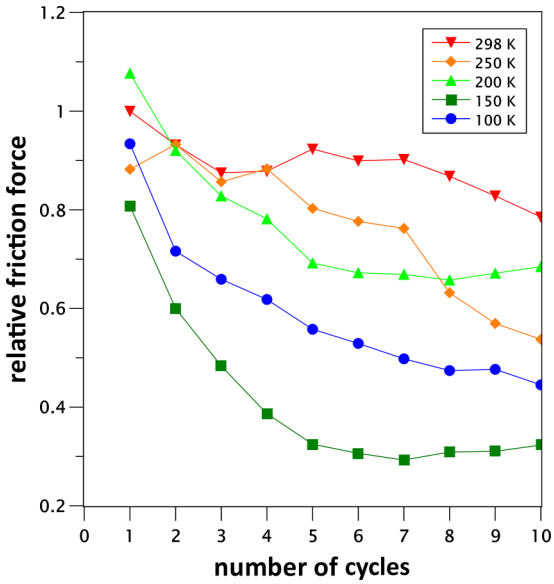

FIG. 10. Normalized friction values obtained on NaCl averaged over one cycle plotted as a function of the cycle number n at different temperatures.

the friction cycles can be observed. This trend is confirmed at other temperatures, as shown in Fig. 10 by the normalized friction values averaged over one cycle plotted as a function of the cycle number n.

On the durable and atomically flat surface of HOPG we only have to consider friction as a thermally activated stick-slip process on a periodic energy surface with relatively low corrugation. However, on an NaCl surface, wear is well known to occur when scanning in contact AFM [34] and indeed confirmed in Fig. 11, which shows topography images before and after ten circulations. Continuous scanning leads to an increased disorder at the interface, and the less commensurate contact so formed can consequently reduce the sliding friction [35]. Atomistic simulations extending earlier results by Wyder *et al.* on this topic [36] may help to shed light on this process.

Figure 10 also shows that the influence of n on the results for NaCl is more pronounced at low temperatures. This is possibly related to self-healing of the damaged surface. Assuming that the process is caused by thermally activated diffusion of the displaced ions, the surface will recover more slowly in this case.

It also worth comparing our results with those reported by Socoliuc *et al.* while repeatedly scraping a KBr(100) surface

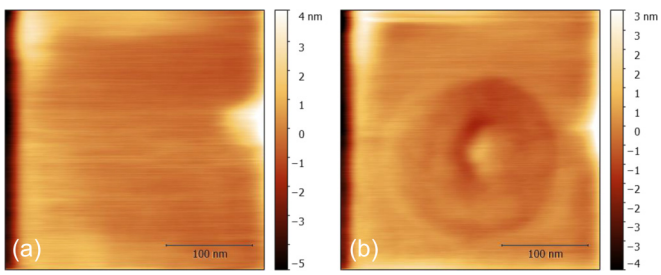

FIG. 11. Topography images of NaCl obtained for a temperature of 200 K (a) before and (b) after ten circulations.

along the main crystallographic axes 256 times [37]. The friction force was found to increase, in parallel with the formation and growth of pits and mounds along the wear groove, hindering the sliding motion. This is not the case here, since the limited scan length (100 nm) did not result in the formation of surface features to be overcome by the tip, which remains rather confined at the first indentation site all the time.

IV. CONCLUSION

To sum up, we used a viable but uncommon approach to analyze the directional dependence of friction, where the relative calibration factors for force detection parallel and perpendicular to the long cantilever axis were extracted from measurements on an amorphous silicon surface by reshaping the resulting ellipse into a circle. In this way, we could investigate the anisotropy of friction on three crystalline surfaces with no need of (physically) rotating the surfaces.

Based on this approach, the dependence of the average friction force on the scan direction as predicted by the Prandtl-Tomlinson model has first been verified for MoS_2. However, although this result appears to be straightforward, it also illustrates the potential extent of tip-sample configurations, since comparable experiments [17,20] have resulted in a twofold symmetry. By measuring on HOPG at different temperatures, we could additionally observe that, if the sample surface is cooled down to 100 K, the tip motion tends to be locked along the crystallographic directions, as seen from the progressive "clustering" of the experimental data points describing the friction dependence on the scan angle in six directions. This effect is also explained by the Prandtl-Tomlinson model, once thermal vibrations are included. The method introduced here could be easily extended to other crystal surfaces with more complex lattice symmetries (e.g., calcite [38] or graphene moiré lattices [39]). Since the friction force is ultimately determined by the tip-surface interaction, the analysis could also be extended to investigate, e.g., the effect of parameters such as the bias voltage applied across the contact (for conductive materials) or the viscosity of a liquid environment (if the tip is fully immersed in the last one liquid environment so that the formation of capillary bridges is excluded). However, one requirement is that the surfaces are not worn off while scanned, as appears to be the case for the NaCl crystal also addressed in this paper. Here, surface defects and wear debris at the interface change the directional dependence of friction from a fourfold symmetry to irregular patterns not compatible with the thermally activated Prandtl-Tomlinson model. Instead, a possible route to understanding the results might be to consider the early stage of abrasive wear by atomistic simulations [36].

ACKNOWLEDGMENTS

D.D. acknowledges financial support provided by the Deutsche Forschungsgemeinschaft (DFG) (Project No. DI917/8-1). E.G. acknowledges the support of the Polish National Science Center (NCN) under Grant No. 2021/43/B/ST5/00705 and the Strategic Program Excellence Initiative (SciMat) of Jagiellonian University under Grant No. U1U/P05/NO/01.05.

[1] C. M. Mate, G. M. Mcclelland, R. Erlandsson, and S. Chiang, Atomic-Scale Friction of a Tungsten Tip on a Graphite Surface, Phys. Rev. Lett. **59**, 1942 (1987).

[2] Q. Li, T. E. Tullis, D. Goldsby, and R. W. Carpick, Frictional ageing from interfacial bonding and the origins of rate and state friction, Nature (London) **480**, 233 (2011).

[3] Y. Shao, T. D. B. Jacobs, Y. Jiang, K. T. Turner, R. W. Carpick, and M. L. Falk, Multibond model of single-asperity tribochemical wear at the nanoscale, ACS Appl. Mater. Interfaces **9**, 35333 (2017).

[4] M. Vorholzer, J. Vilhena, R. Perez, E. Gnecco, D. Dietzel, and A. Schirmeisen, Temperature Activates Contact Aging in Silica Nanocontacts, Phys. Rev. X **9**, 041045 (2019).

[5] M. Vorholzer, D. Dietzel, E. Cihan, and A. Schirmeisen, Shear-assisted contact aging of single-asperity nanojunctions, Phys. Rev. B **105**, 195401 (2022).

[6] L. Prandtl, Ein Gedankenmodell zur kinetischen Theorie der festen Körper, Z. Angew. Math. Mech. **8**, 85 (1928).

[7] U. D. Schwarz and H. Hölscher, Exploring and explaining friction with the Prandtl-Tomlinson model, ACS Nano **10**, 38 (2016).

[8] M. Dienwiebel, G. S. Verhoeven, N. Pradeep, J. W. M. Frenken, J. A. Heimberg, and H. W. Zandbergen, Superlubricity of Graphite, Phys. Rev. Lett. **92**, 126101 (2004).

[9] A. Socoliuc, R. Bennewitz, E. Gnecco, and E. Meyer, Transition from Stick-Slip to Continuous Sliding in Atomic Friction: Entering a New Regime of Ultralow Friction, Phys. Rev. Lett. **92**, 134301 (2004).

[10] S. N. Medyanik, W. K. Liu, I.-H. Sung, and R. W. Carpick, Predictions and Observations of Multiple Slip Modes in Atomic-Scale Friction, Phys. Rev. Lett. **97**, 136106 (2006).

[11] E. Gnecco, L. Agmon, and R. Berkovich, Friction and chaos: Influence of the damping coefficient on atomic-scale stick-slip on hexagonal crystal lattices, Phys. Rev. B **105**, 235427 (2022).

[12] K. B. Jinesh and J. W. M. Frenken, Capillary Condensation in Atomic Scale Friction: How Water Acts like a Glue, Phys. Rev. Lett. **96**, 166103 (2006).

[13] I. Barel, A. E. Filippov, and M. Urbakh, Formation and rupture of capillary bridges in atomic scale friction, J. Chem. Phys. **137**, 164706 (2012).

[14] E. Riedo, F. Levy, and H. Brune, Kinetics of Capillary Condensation in Nanoscopic Sliding Friction, Phys. Rev. Lett. **88**, 185505 (2002).

[15] S. G. Balakrishna, A. S. de Wijn, and R. Bennewitz, Preferential sliding directions on graphite, Phys. Rev. B **89**, 245440 (2014).

[16] Y. Song, J. Wang, Y. Wang, M. Urbakh, Q. Zheng, and M. Ma, Directional anisotropy of friction in microscale superlubric graphite/*h*BN heterojunctions, Phys. Rev. Mater. **5**, 084002 (2021).

[17] X. Cao, X. Gan, H. Lang, K. Yu, S. Ding, Y. Peng, and W. Yi, Anisotropic nanofriction on MoS_2 with different thicknesses, Tribol. Int. **134**, 308 (2019).

[18] A. Khomenko, M. Zakharov, and B. N. J. Persson, Frictional anisotropy of Al, Pt, and Pd nanoparticles on a graphene substrate, Tribol. Lett. **67**, 113 (2019).

[19] G. Fessler, A. Sadeghi, T. Glatzel, S. Goedecker, and E. Meyer, Atomic friction: Anisotropy and asymmetry effects, Tribol. Lett. **67**, 59 (2019).

[20] M. R. Vazirisereshk, K. Hasz, R. W. Carpick, and A. Martini, Friction anisotropy of MoS_2: effect of tip-sample contact quality, J. Phys. Chem. Lett. **11**, 6900 (2020).

[21] A. S. de Wijn, (In)commensurability, scaling, and multiplicity of friction in nanocrystals and application to gold nanocrystals on graphite, Phys. Rev. B **86**, 085429 (2012).

[22] D. Dietzel, A. de Wijn, M. Vorholzer, and A. Schirmeisen, Friction fluctuations of gold nanoparticles in the superlubric regime, Nanotechnology **29**, 155702 (2018).

[23] A. S. de Wijn, C. Fusco, and A. Fasolino, Stability of superlubric sliding on graphite, Phys. Rev. E **81**, 046105 (2010).

[24] Z. Liu, J. Yang, F. Grey, J. Z. Liu, Y. Liu, Y. Wang, Y. Yang, Y. Cheng, and Q. Zheng, Observation of Microscale Superlubricity in Graphite, Phys. Rev. Lett. **108**, 205503 (2012).

[25] E. Gnecco, R. Bennewitz, T. Gyalog, C. Loppacher, M. Bammerlin, E. Meyer, and H. J. Güntherodt, Velocity Dependence of Atomic Friction, Phys. Rev. Lett. **84**, 1172 (2000).

[26] Y. Sang, M. Dube, and M. Grant, Thermal Effects on Atomic Friction, Phys. Rev. Lett. **87**, 174301 (2001).

[27] R. W. Carpick and M. Salmeron, Scratching the surface: fundamental investigations of tribology with atomic force microscopy, Chem. Rev. **97**, 1163 (1997).

[28] *Fundamentals of Friction and Wear on the Nanoscale*, 2nd ed., edited by E. Gnecco and E. Meyer, NanoScience and Technology Series (Springer, Cham, Switzerland, 2014).

[29] E. Gnecco, Quasi-isotropy of static friction on hexagonal surface lattices, EPL (Europhys. Lett.) **91**, 66008 (2010).

[30] P. Steiner, R. Roth, E. Gnecco, A. Baratoff, S. Maier, T. Glatzel, and E. Meyer, Two-dimensional simulation of superlubricity on NaCl and highly oriented pyrolytic graphite, Phys. Rev. B **79**, 045414 (2009).

[31] M. P. Allen and D. J. Tildesley, *Computer Simulation of Liquids*, 2nd ed. (Oxford University Press, Oxford, 2017).

[32] O. Y. Fajardo, E. Gnecco, and J. J. Mazo, Anisotropy effects and friction maps in the framework of the 2d PT model, Phys. B (Amsterdam) **455**, 44 (2014).

[33] See Supplemental Material at http://link.aps.org/supplemental/10.1103/PhysRevB.107.195438 for simulated friction-vector plots for NaCl.

[34] W. Wang, D. Dietzel, and A. Schirmeisen, Thermal Activation of Nanoscale Wear, Phys. Rev. Lett. **126**, 196101 (2021).

[35] B. Luan and M. O. Robbins, The breakdown of continuum models for mechanical contacts, Nature (London) **435**, 929 (2005).

[36] U. Wyder, A. Baratoff, E. Meyer, L. N. Kantorovich, J. David, S. Maier, T. Filleter, and R. Bennewitz, Interpretation of atomic friction experiments based on atomistic simulations, J. Vac. Sci. Technol., B: Microelectron. Nanometer Struct.–Process., Meas., Phenom. **25**, 1547 (2007).

[37] A. Socoliuc, E. Gnecco, R. Bennewitz, and E. Meyer, Ripple formation induced in localized abrasion, Phys. Rev. B **68**, 115416 (2003).

[38] C. M. Pina, R. Miranda, and E. Gnecco, Anisotropic surface coupling while sliding on dolomite and calcite crystals, Phys. Rev. B **85**, 073402 (2012).

[39] N. Chan, S. G. Balakrishna, A. Klemenz, M. Moseler, P. Egberts, and R. Bennewitz, Contrast in nanoscale friction between rotational domains of graphene on Pt(111), Carbon **113**, 132 (2017).